A Novel Heme and Peroxide-Dependent Tryptophan-Tyrosine Cross-link in a Mutant of Cytochrome c Peroxidase

B. Bhaskar[1,4], Chad E. Immoos[3,6], Hideaki Shimizu[1,4,5], Filip Sulc[3], Patrick J. Farmer[3], Thomas L. Poulos[1,2,4]

[1] Department of Molecular Biology & Biochemistry, [2] Department of Physiology & Biophysics, [3] Department of Chemistry, and the [4] Program in Macromolecular Structure, University of California, Irvine, CA 92697-3900

[5] Present address: Molecular Neuropathology Group, RIKEN Brain Science Institute, 2-1 Hirosawa, Wako-shi, Saitama 351-0198, JAPAN

[6] Present address : Department of Chemistry, P.M. Gross Chemical Laboratories, Duke University, Durham, NC 27708

To whom the correspondence should be addressed to:
Thomas L. Poulos,
Department of Molecular Biology and Biochemistry,
University of California-Irvine, Irvine CA 92697-3900
Phone: (949)-824-7020 : *FAX*: (949)-824-3280 : *E-mail*: poulos@uci.edu

Abstract

The crystal structure of a cytochrome *c* peroxidase mutant where the distal catalytic His52 is converted to a Tyr reveals that the tyrosine side chain forms a covalent bond with the indole ring nitrogen of Trp51. We hypothesize that this novel bond results from peroxide activation by the heme iron followed by oxidation of Trp51 and Tyr52. This hypothesis has been tested by incorporation of a redox-inactive Zn-protoporphyrin into the protein, and the resulting crystal structure shows the absence of a Trp51-Tyr52 cross-link. Instead, the Tyr52 side chain orients away from the heme active site pocket, which requires a substantial rearrangement of residues 72-80 and 134-144. Additional experiments where heme-containing crystals of the mutant were treated with peroxide support our hypothesis that this novel Trp-Tyr cross-link is a peroxide-dependent process mediated by the heme iron.

Keywords

Cytochrome *c* peroxidase; X-ray crystal structure; Fe-containing heme; Zn-containing protoporphyrin IX; oxygen radical; tryptophan-tyrosine cross-link; Trp cation radical.

Abbreviations

CcP, cytochrome *c* peroxidase; CcO, cytochrome *c* oxidase; cyt. *c*, reduced horse heart or yeast cytochrome *c*; EDTA, ethylenediaminetetraacetic acid; MPD, 2-methyl-2,4-pentanediol; KPB, potassium phosphate buffer; M_r, relative molecular mass; IPTG, isopropylthio-β-galactoside

Introduction

Baker's yeast (*Saccharomyces cerevisiae*) cytochrome *c* peroxidase (CcP) [ferrocytochrome *c*: hydrogen peroxide: oxidoreductase, EC 1.11.1.5] is a mitochondrial intermembrane space protein of M_r = 32,240 daltons[1] where it most likely functions to protect the organism against high concentrations of hydrogen peroxide[2]. CcP catalyzes the two-electron reduction of peroxide to water in a multi-step reaction cycle as follows:

$$\underset{\textit{Resting State}}{Fe^{3+}\ Trp} + H_2O_2 \rightarrow \underset{\textit{Compound I}}{Fe^{4+}\text{-}O\ Trp^{\bullet+}} + H_2O$$

$$\underset{\textit{Compound I}}{Fe^{4+}\text{-}O\ Trp^{\bullet+}} + \text{cyt. } c\ (Fe^{2+}) \rightarrow \underset{\textit{Compound II}}{Fe^{4+}\text{-}O\ Trp} + \text{cyt. } c\ (Fe^{3+})$$

$$\underset{\textit{Compound II}}{Fe^{4+}\text{-}O\ Trp} + \text{cyt. } c\ (Fe^{2+}) \rightarrow \underset{\textit{Resting State}}{Fe^{3+}\ Trp} + \text{cyt. } c\ (Fe^{3+}) + H_2O$$

CcP first reacts with peroxide to give a stable intermediate where the two oxidizing equivalents of peroxide are stored on the iron as Fe^{4+}-O and as an amino acid free radical located on Trp191[3-6]. This oxidized state, designated *Compound I*, has a half-life of several hours in the absence of reductant[7]. *Compound I* then is reduced by cyt. *c* (Fe^{2+}) back to the resting state in two successive one-electron transfer reactions. One remarkable aspect of this electron transfer reaction is that the heme edges of the redox partners remain separated by no less than 18 Å, as revealed by the crystal structure of the non-covalent complex [8].

A unique feature of the CcP reaction cycle is the formation of a stable Trp cationic radical in *Compound I*[4]. Trp191 lies parallel to and in contact with the proximal heme ligand, His175, situated just beneath the heme. Trp191 is also essential for CcP activity and critical for long-distance electron transfer reaction from cyt. *c* to CcP[9-12]. Thus, the Trp191 radical constitutes an electron transfer gate that allows the controlled reduction of peroxide, a two-electron oxidant, by cyt. *c*, a one-electron reductant. Although details of

how electrons are transferred from reduced cyt. *c* to CcP are unclear, the crystal structure of CcP-cyt. *c* complex does indicate that cyt. *c* binds near the 190-195 loop region of CcP[8]. The CcP-cyt. *c* co-crystal structure[8] together with a wealth of biochemical data indicates that each electron delivered from ferrocyt. *c* is accepted by the Trp^{191} cationic radical[13,14] which explains why Trp191 is essential for activity[15].

In the present investigation we have made a mutant variant of CcP by replacing the distal His^{52}, a residue which functions as an acid-base catalyst in the reaction with peroxide**[16]**, to Tyr as part of a project to engineer novel enzyme activities into CcP. The crystal structure of H52Y reveals an unprecedented Trp-Tyr covalent cross-link. Structural details, a proposed mechanism of covalent cross-link formation, and its implications are the topics of this paper.

Results

Overall protein fold and comparison with the wild-type CcP:

The overall structure of CcP is shown in **Fig. 1** together with key regions relevant to this study highlighted. The first data set analyzed using chunky crystals, where the cross-link was first observed, is designated H52Y1. All essential features of the secondary structure of H52Y1 resembled that of wild-type CcP. However, dramatic and unexpected changes were observed in the active site. The initial electron density maps showed continuous density between the Trp51 indole ring NE1 atoms and CE1 of Tyr52 (**Fig. 2A**). When non-bonded contact restraints between Trp51 and Tyr52 were not included in the refinement, the indole ring was oriented such that its NE1 atom was located less than 1.6 Å from CE1 atom of phenyl ring of Tyr52. This distance is, within experimental error, what is expected for a C-N covalent bond (1.48 Å)[17] and precludes a non-covalent interaction. As refinement progressed $2F_o$-F_c composite omit maps continually revealed a clear connection between Trp51 and Tyr52 with electron density as strong as any other covalent bond along the main chain.

In addition to the Trp51-Tyr52 cross-link, there also were other smaller changes in the active site. The cross-linked mutant is hexa-coordinate with a water molecule serving as the sixth heme ligand at a distance of 1.95 Å from the iron. Arg48 (**Fig. 1**), which is thought to participate in the catalytic cleavage of the peroxide O-O bond[16], occupies a single '*out*' conformation towards the heme propionates while in wild-type CcP Arg[48] occupies both the *'out'* conformation and *'in'* conformation closer to the heme iron.

Structure of Zn-porphyrin H52Y:

It seemed likely that the cross-link was the result of a redox-linked process involving the heme iron and peroxide or other contaminating oxidants. To test this hypothesis apo-CcP was reconstituted with the redox-inactive Zn-porphyrin and crystallized. The Zn-porphyrin crystals grew in both the chunky and plate forms. Both forms are in space group $P2_12_12_1$ with similar unit cell dimensions (**Table I**). The data set used to solve the structure employing plate crystals is designated ZnH52Y (**Table I**).

As expected the Trp51-Tyr52 cross-link did not form in ZnH52Y (**Fig. 2F**). Since the cross-link did not form, the Tyr52 side chain cannot remain oriented into the active site since this would result in steric clashes with Trp51. Therefore, the Tyr52 side chain rotates ≈ 60° away from the active site into the '*open*' conformation, which leads to substantial structural changes. To make room for the new position of Tyr52 requires the disruption of two helices between residues 70-82 and an adjacent segment of polypeptide involving residues 134-144 (**Fig. 3**). In this '*open*' position the side chain Tyr-OH donates a 2.7 Å hydrogen bond to the side chain OD2 atom of Asp140. The conformational change involving residues 70-82 results in the phenyl ring side chains of residues 73, 77 and 89 coming together to form a hydrophobic patch which may in part balance the stability lost owing to disruption of helices. This change in conformation also has been observed in another mutant structure of CcP (1DSE)[18]. In this case, the proximal His175 ligand was replaced by Gly which allows free imidazole to coordinate as a proximal ligand. When phosphate is bound in the distal pocket, His52 must move and adopts a conformation virtually identical to the *'open'* conformation of Tyr52. Moreover, the resulting structural changes in the surrounding protein are essentially the same as we observe in the H52Y mutant.

Other changes in the active site are relatively small. The Zn^{2+} atom still coordinates with His175 at a distance of 2.12 Å which is 0.07 Å longer than in wild-type CcP. Although a water molecule is situated in the distal pocket this water is not coordinated to the Zn^{2+} as indicated by the lack of continuous density with the Zn^{2+} and a Zn-water distance of ~ 3.7 Å. We also observed a large lobe of electron density extending off the δ-*meso* edge of the porphyrin indicating a covalent C-O bond (**Fig. 4**). We suspect this modification might be the result of the enhanced photosensitivity of Zn-protoporphyrhin IX leading to photo-oxidation of the relatively labile δ-*meso* carbon.

Structure of '*open*' form H52Y:

At this stage crystals of another preparation of H52Y were grown under similar conditions as mentioned in "*Materials and Methods*" which yielded the chunky and plate form crystals. Crystal structures of both (H52Y6 and PLH52Y) were solved. Both these structures revealed the '*open*' conformation of Tyr52 very similar to the Zn-porphyrin

structure without formation of the cross-link (**Figs. 2 B & D**). We then were left with the question of why H52Y1 showed the Trp51-Tyr52 cross-link while both H52Y6 and PLH52Y did not have the cross-link. The main difference is that H52Y1 was crystallized from an older batch of MPD. It is well known that MPD can generate breakdown products including peroxides that could provide the oxidizing equivalents required to form the cross-link.

Structures of Peroxide Treated Crystals

Unfortunately the older batch of MPD no longer is available and hence, this hypothesis cannot be directly tested. Nevertheless, if peroxide is responsible for the cross-link then treating H52Y crystals with peroxide should show formation of the cross-link. Crystals were soaked in mother liquor (35% MPD in 50 mM KPB, pH 6.0) containing 10 mM hydrogen peroxide for 1 h followed by washing in peroxide-free mother liquor to remove excess peroxide before X-ray data collection. A crystal from the same drop used to obtain the H52Y6 structure was treated with peroxide, data collected, and the structure solved. This structure, designated H52Yper, clearly showed formation of the cross-link (**Fig. 2C**). Crystals containing Zn-porphyrin crystals could withstand a freeze-thaw cycle so here it was possible to collect a set of data, thaw the crystal, treat with peroxide, and collect a second data set. A comparison of the ZnH52Y (peroxide-free) and ZnH52Yper (peroxide-treated) electron density maps (**Figs. 2 F & G**) clearly show that the cross-link does not form and that Tyr52 adopts the *'out'* conformation with or without peroxide treatment. These several structures show that both peroxide involvement and presence of heme iron are required to form the cross-link.

Discussion

There is a growing list of novel covalent linkages and post-translational modifications known to be critical in forming enzyme active sites. The methionine sulfone found in the active site of catalase from *Proteus mirabilis*[19], cysteine sulfonic acid in NADH peroxidase from *Streptococcus faecalis*[20], internal cyclization of the peptide backbone with the accompanying oxidation of the C_α-C_β bond of Tyr66 in the green fluorescent protein (GFP)[21,22] and pyrrolysine in *Methanosarcina barkeri*[23] are all recent findings. There also are several examples of cross-links involving aromatic residues. These include the copper coordinated His240-Tyr244 cross-link at the O_2-activating heme Fea_3-Cu_B center in subunit I of cytochrome *c* oxidase[24-27], a covalent bond between the N_δ of the imidazole ring of His392 and the C_β of the essential Tyr415 in *Escherichia coli* catalase HPII[28], an unexpected covalent linkage between Tyr272 and Cys228 in galactose oxidase of a fungus, *Dactylium dendroides*[29], and a 2,4,5-trihydroxyphenylalanine quinone in amine oxidase[30]. The most recent example is a Met-Tyr-Trp cross-link in a catalase-peroxidase[31]. In this case the Tyr-Trp cross-link is between 2 aromatic carbon atoms. Our present findings thus represent the second example of a Trp-Tyr cross-link but differs since the indole ring N atom of the Trp participates in the cross-link.

Our results clearly show that both the iron and peroxide are required to form the cross-link. However, several lines of evidence indicate that the normal *Compound I* consisting of Fe(IV)-O and the Trp191 cationic radical is not the intermediate responsible for the Trp-Tyr cross-link. Changing His52 to other residues in CcP decreases the rate of normal *Compound I* formation by 5 orders of magnitude[32]. Indeed, addition of H_2O_2 to the H52Y mutant does not generate the characteristic Fe(IV)-O spectrum while the EPR spectrum indicates only 5% oxidation of Trp191 (data not shown). Driving force considerations also do not favor sequential one electron oxidations by Fe(IV)-O and a neighboring organic radical as in the normal peroxidase reaction. The CcP *Compound I* potential is 0.754 V[33], while the oxidation potentials of the deprotonated Trp and Tyr anions are 1.01 and 0.96 V, respectively[34]. As with the Trp191, these potentials may be significantly

altered by protein environments although in native CcP there is no evidence for Trp51 oxidation by either Fe(IV)-O or the Trp191 cationic radical.

There also are fundamental difficulties in forming a Trp-Tyr cross-link by sequential one-electron oxidations. Aromatic radicals are inert to nucleophilic attack and coupling reactions are typically *via* radical-radical combinations. While Trp and Tyr are among the most susceptible to radical reactions[35], a limiting factor is the short lifetime of such radicals. Thus concurrent oxidation at both sites is suggested, limiting the possible mechanisms of cross-link formation.

Cross-link formation *via* a peroxidic intermediate is consistent with these requirements, as shown in **Fig. 5**. In this mechanism, an Fe-bound peroxide generates both Trp and Tyr radicals by H-atom abstraction, avoiding the need for Compound 1 formation. Modeling an Fe-bound peroxide in the active site of the mutant shows that the Tyr52 -OH group can approach close enough to the O^{β}-atom of peroxide for H atom abstraction giving the phenol radical. Similarly, the indole -NH group of Trp51 is within H-bonding distance of the iron-bound O^{α} atom thus enabling H-atom abstraction and formation of the indole radical. Owing to resonance stabilization, the electron deficient center of Tyr52 is delocalized over the phenol ring system thus enabling reaction with the nearby Trp51 radical.

The most unusual aspect of the Trp-Tyr mutant structure is the cross-link C-N bond itself. Aromatic couplings of indoles most frequently occur at an indolic C rather than N atom. Likewise, it would be expected that the N-alkyl bond would remain approximately planar to the aromatic ring in order to maintain the sp^2 hybridization at the indolic N. In the Trp-Tyr covalent cross-link, the N is highly pyramidalized, with the $NE1_{Trp}$-$CE1_{Tyr}$ bond bent $\approx 64°$ from the aromatic plane. Pyramidalized indolic N-alkyl bonds are precedented, most notably in the structure of rebeccamycin, an N-glycosylated indolocarbazole, with an indolic N to sugar bond ca. 27^{o} out of the aromatic plane[36] and bent N-C bonds are seen in synthetic analogues as well[37]. To our knowledge, the Trp-Tyr mutant has by far the largest deformation of an alkylated indole yet observed, and is unprecedented in known protein structures.

To understand the variation of strain energy with bending of the $NE1_{Trp}$-$CE1_{Tyr}$ linkage, a series of calculations were done at the semi-empirical level using AM1 methods on an analogously coupled indole-arene model (**Fig. 6**). The gas-phase energies were calculated as the N-C bond was varied from 0° to 60° relative to the dihedral angle of the indole and arene rings (**Fig. 6**). Deformations up to 30°, as seen in rebeccamycin, are predicted to have a small energy cost of ca. 2 kcal/mol. The deformation in the Trp-Tyr cross-link is about 60° which, according to **Fig. 6**, gives a strain energy of 9.8 kcal/mol. This energy cost due to conformational constraints in formation of the C-N bond must be counterbalanced by inherent energies within the folded protein.

Although the Trp-Tyr cross-link is unique, it is comparable to the His-Tyr cross-link in cytochrome *c* oxidase[26] and catalase HPII[28] and Cys-Tyr cross-link in galactose oxidase[29]. In the cases of cytochrome *c* oxidase and catalase, one of the cross-linked side chains is a metal ligand which suggests a metal-dependent redox process as part of the cross-link chemistry similar to what we observe in the present study. CcP thus provides an excellent model system for studying cross-linking chemistry required for critical biological processes, especially since we have shown that it is relatively easy to control formation of the cross-link. This also raises the possibility that nearly any His-Tyr or Trp-Tyr pair that are directly connected along the primary sequence, especially in an α-helix, or are similarly juxtaposed in three-dimensional space, may be susceptible to cross-linking given a suitable redox environment.

Materials and Methods

Materials: Enzymes and reagents for site-directed mutagenesis were purchased from Roche Molecular Biochemicals and New England Biolabs Inc. (Beverly, MA). Stratagene Quickchange Mutagenesis Kit (Cat # 200516) was purchased from Stratagene Inc., La Jolla, CA. Chromatography columns and resins, media and Na^+/K^+ free Tris base were purchased from Amersham-Pharmacia Biotech. Zn-protoporphyrin IX was purchased from Frontier Scientific Porphyrin Products, Logon, Utah. IPTG was purchased from USB Corporation, Cleveland, OH. 2-methyl-2,4-pentanediol (MPD) and ion free phosphoric acid were purchased from Aldrich Chemicals. All other chemicals were molecular biology grade or better and were purchased from Sigma or Fisher.

Site-directed mutagenesis: Oligonucleotide-directed mutagenesis experiments were performed on pT7-7 vector that contained the wild-type CcP gene using the Stratagene Quickchange Mutagenesis Kit (Cat # 200516) with the help of appropriate primers to obtain the desired mutation. To change the distal His^{52} to Tyr the following sense and anti-sense primers were purchased from Operon Technologies Inc., Alameda, CA.

5' CGTCTTGCTTGGTACACTTCAGGGACC 3'

5' GGTCCCTGAAGTGTACCAAGCAAGACG 3'

Mutagenesis was carried out using *Pfu Turbo* DNA polymerase and a temperature cycler. The oligonucleotide primers, each complementary to opposite strands of the vector, are extended during temperature cycling by *Pfu Turbo* DNA polymerase. Incorporation of oligonucleotide primers generates a mutated plasmid with staggered nicks. Following temperature cycling, the product was subjected to *Dpn I* endonuclease digestion to digest methylated and hemi-methylated parental DNA and to select for mutation-containing synthesized DNA. The nicked DNA vector with desired mutation is transformed into *Epicurian XL1-Blue* supercompetent cells. The small amount of starting DNA template, high fidelity of *Pfu Turbo* DNA polymerase and low number of thermal cycles all contribute to high mutation frequency. The mutant clones analyzed by restriction analysis and automated DNA sequencing was done at the UCI DNA sequencing core facility to confirm the desired mutation. This mutant variant protein was designated H52Y.

Protein expression and purification: Mutant CcP (H52Y) protein was expressed under the control of T7 promoter in *Escherichia coli BL21(DE3)* cells induced at A_{600} of 1.2-1.5 with 750 •M IPTG. Proteins were purified as previously described by Fishel *et al.*[38] and Choudhury *et al.*[39] with minor modification. After gel filtration on a Sephadex G-75 column and heme (Fe^{3+}-protoporphyrin IX) incorporation into the apo-CcP by standard pH shift, the holo-CcP was separated by DEAE-Sephacel anion exchange chromatography. Since this mutant variant did not crystallize upon dialysis against distilled water, protein was stored in 100 mM potassium phosphate buffer (KPB), pH 6.0. For incorporating Zn^{2+}-protoporphyrin IX into the mutant protein, the crude lysate after gel filtration on a Sephadex G-75 column gave a mixture of apo- and holo-fractions of CcP. Apo-CcP fraction was separated from the small amount of holo-CcP by HiTrap-Q anion exchange chromatography using Amersham-Pharmacia Biotech FPLC system. Stepping the gradient first to 80 mM, then to 130 mM potassium phosphate and finally a linear gradient of 130-500 mM KPB, pH 6.0 separated apo-CcP from holo-CcP. Apo-CcP was extensively dialyzed against 100 mM KPB, pH 7.25 before Zn^{2+}-protoporphyrin IX incorporation. After dissolving Zn^{2+}-protoporphyrin IX in 0.1 N NaOH, it was diluted by the addition of 100 mM KPB, pH 7.25. This mixture was added to the dialyzed apo-CcP, followed by incubation overnight in the cold on an *end to end* shaker. Since Zn^{2+}-protoporphyrin IX is photosensitive, all operations were performed in the dark. This mixture was extensively dialyzed against 50 mM and then 20 mM KPB, pH 6.0. Zn^{2+}-protoporphyrin incorporated CcP was then purified by DEAE-Sephacel anion exchange chromatography. Zn^{2+}-protoporphyrin containing CcP was stored in 100 mM KPB, pH 6.0 after dialysis against the same buffer. Mutant CcP concentrations were estimated spectrophotometrically using an extinction coefficient at 408 nm (ε_{408}) of 96,000 M^{-1} cm^{-1}.

Crystallization: Diffraction quality crystals of Fe-containing as well as Zn-porphyrin H52Y were prepared in 30% 2-methyl-2,4-pentanediol (MPD), 50 mM potassium phosphate, pH 6.0 (KPB) or 50 mM Tris-phosphate, pH 6.0 according to Edwards and Poulos[40] as later modified by Sundaramoorthy *et al.*[41].(~D6ops containing 500 •M (~16 mg/mL) protein, 50 mM KPB or tris-phosphate, pH 6.0 and 18% MPD were equilibrated against 30% MPD at 4°C. Drops were touch seeded from previously grown CcP crystals

and incubated at 4°C until crystal growth was complete (2-4 days). 0.2 mm crystals from touch seeding were used for X-ray data collection. This smaller size crystal was necessary for better cryogenic freezing and to avoid twinning during crystal growth. Crystals were mounted in nylon loops and frozen directly in a cryo-stream held at 121 K. The Fe-containing H52Y crystallized in two forms, chunky (regular wild-type like) and as plates, both of them in the space group $P2_12_12_1$, but with different unit cell dimensions (**Table I**). The Zn-porphyrin H52Y also crystallized in the same two forms belonging to space group $P2_12_12_1$, but both forms crystallized with similar unit cell dimensions (**Table I**).

To form this Trp-Tyr cross-link in the crystal, crystals were soaked in mother liquor (35% MPD, 50 mM Tris-phosphate, pH 6.0) containing 10 mM hydrogen peroxide for 1 h followed by soaking in 35% MPD in 50 mM Tris-phosphate, pH 6.0 to remove excess peroxide before using the crystal for X-ray data collection. X-ray diffraction data of resting and peroxide-treated crystals could be obtained from the same crystals for Zn-porphyrin H52Y since one form of these crystals could withstand a freeze-thaw cycle. After data collection, crystals were thawed in mother liquor (35% MPD, 50 mM Tris-phosphate, pH 6.0) containing 10 mM hydrogen peroxide for 1 h followed by soaking in 35% MPD in 50 mM Tris-phosphate, pH 6.0 to remove excess peroxide followed by freezing and data collection.

X-ray data collection and reduction: All X-ray diffraction data of resting state and *Compound I* of H52Y were collected at cryogenic temperatures in a stream of liquid nitrogen. Since CcP crystals are grown from solutions containing MPD, there was no need for the addition of cryo-solvents. All X-ray intensity data of all forms of heme and Zn-porphyrin crystals were obtained '*in-house*' using a Rigaku *R-AXIS IV* image plate system with a Rigaku rotating anode operating at 100 mA and 50 kV equipped with Osmic optics. A single crystal was used for each dataset. Initial image processing, indexing, and integration were performed with *DENZO* (version 1.9.1), and the integrated data were averaged and scaled with *SCALEPACK*[42]. The X-ray intensity data from Zn-porphyrin containing H52Y crystals were processed, indexed, integrated and scaled with *XENGEN*[43]. Statistics from data processing of all datasets are listed in **Table I**.

Structure solution and refinement: The H52Y mutant crystallized in two forms: the usual chunky crystals and a new form shaped like plates. The regular chunky crystal form of H52Y, which we have termed the H52Y1, is isomorphous with wild-type crystals[44]. The structure of resting wild-type CcP refined to 1.2 Å using data collected at the Stanford Synchrotron Research Laboratory (SSRL, unpublished) was the starting model for refinement. Rigid body refinement (RBR) was followed by slow-cool simulated annealing minimization with *CNS* (version 1.1) to remove phase bias and the remaining refinement cycles were performed using conjugated gradient minimization and *B*-factor refinement with *CNS* (version 1.1)[45]. Approximately 5% of the data was omitted from the refinement and used as a test set[46] and the same set of test reflections was maintained throughout refinement. Individual but restrained *B*-factors were refined in *CNS* (version 1.1)[45]. To obtain parameters for the novel C-N bond between the mutant Tyr52 side chain and Trp51, a small molecule model of the cross-link was energy minimized using semi-empirical calculations and the bond parameters derived from these calculations were used as restraints in *CNS*. These calculations gave a C-N bond distance of 1.45 Å. $2F_o$-F_c and F_o-F_c electron density maps were calculated in *CNS* (version 1.1) and used for model corrections in *TOM* (version 3.0), a variant of *FRODO*[47]. Water molecules were retained in the model if they returned in $2F_o$-F_c and F_o-F_c electron density maps and obeyed hydrogen bonding criteria. Iterative cycles of model building in *TOM* (version 3.0) were followed by conjugated gradient minimization and *B*-factor refinement in *CNS* (version 1.1)[45]. Final model building were based on $2F_o$-F_c composite omit maps.

Since the plate like crystals of Fe-containing H52Y and ZnH52Y were not isomorphous with chunky crystals, it was necessary to use molecular replacement, *AMoRe*[48] with data obtained from plate crystals. The most successful search model consisted of a full molecule of the H52Y structure derived from chunky crystals. The rotation search at 20-5 Å was followed by translation searches of all the rotation solutions at the same resolution. The top solution of translation search for space group $P2_12_12_1$ was followed by rigid body refinement (RBR) at 20-5 Å in *AMoRe*[48]. The coordinates and structure factors of the top solution after RBR were taken through refinement in *CNS* (version 1.1) [45]. Rigid body refinement (RBR) in *CNS* (version 1.1) at 50-2.5 Å was followed by the

same refinement protocol described earlier. Figures were prepared with *MolScript*[49] *BobScript*[50] and *Raster3D*[51].

Coordinates: PDB Coordinates have been deposited in the Protein Data Bank (accession codes **1MK8**, **1MKQ**, **1MKR** and **1ML2**).

Acknowledgements

The authors wish to thank Dr. Andy J. Howard, IMCA-CAT, Advanced Photon Source, Argonne National Laboratory, Argonne, IL 60439 for processing of the Zn-porphyrin data. The authors also thank Prof. David Van Vranken for discussions and assistance in computational modeling. This research was supported by the National Science Foundation (PJF CHE- 0100774) and the National Institutes of Health (TLP GM 42614). Chad Everet Immoos acknowledges a graduate fellowship from the UC Toxic Substances Research and Teaching Program.

References

1. Yonetani, T. & Ohnishi, T. (1996). CcP, a mitochondrial enzyme of yeast. *J. Biol. Chem.* **241**, 2983-2984.
2. Chance, B., Devault, D., Legallais, V., Mela, L. & Yonetani, T. (1967). *Kinetics of electron transfer reactions in biological systems*. Fast Reactions and Primary Processes in Chemical Kinetics, (Claesson, S., Ed.), Interscience, New York.
3. Erman, J. E., Vitello, L. B., Mauro, J. M. & Kraut, J. (1989). Detection of an oxyferryl porphyrin π-cation-radical intermediate in the reaction between hydrogen peroxide and a mutant yeast cytochrome *c* peroxidase. Evidence for tryptophan-191 involvement in the radical site of compound I. *Biochemistry* **28**, 7992-7995.
4. Sivaraja, M., Goodin, D. B., Smith, M. & Hoffman, B. M. (1989). Identification by *ENDOR* of Trp191 as the free-radical site in cytochrome *c* peroxidase compound ES. *Science* **245**, 738-740.
5. Houseman, A. L., Doan, P. E., Goodin, D. B. & Hoffman, B. M. (1993). Comprehensive explanation of the anomalous EPR spectra of wild-type and mutant cytochrome *c* peroxidase compound ES. *Biochemistry* **32**, 4430-4443.
6. Huyett, J. E., Doan, P. E., Gurbiel, R., Houseman, A. L. P., Sivaraja, M., Goodin, D. B. & Hoffman, B. M. (1995). Compound ES of cytochrome *c* peroxidase contains a Trp π-cation radical - characterization by CW and pulsed Q-band *ENDOR* spectroscopy. *J. Amer. Chem. Soc.* **117**, 9033-9041.
7. Erman, J. E. & Yonetani, T. (1975). The oxidation of cytochrome *c* peroxidase by hydrogen peroxide. Characterization of products. *Biochim. Biophys. Acta* **393**, 343-349.
8. Pelletier, H. & Kraut, J. (1992). Crystal structure of a complex between electron transfer partners, cytochrome *c* peroxidase and cytochrome *c*. *Science* **258**, 1748-1755.
9. Bonagura, C. A., Sundaramoorthy, M., Pappa, H. S., Patterson, W. R. & Poulos, T. L. (1996). An engineered cation site in cytochrome *c* peroxidase alters the reactivity of the redox active tryptophan. *Biochemistry* **35**, 6107-6115.
10. Hahm, S., Green, L., Durham, B. & Millett, F. (1993). Reaction of cytochrome *c* with the radical in cytochrome *c* peroxidase compond I. *J. Amer. Chem. Soc.* **115**, 3372-3373.
11. Hahm, S., Miller, M. A., Geren, L., Kraut, J., Durham, B. & Millett, F. (1994). Reaction of horse cytochrome *c* with the radical and the oxyferryl heme in cytochrome *c* peroxidase compound I. *Biochemistry* **33**, 1463-1480.
12. Pappa, H. S., Tajbaksh, S., Saunders, A. J., Pielak, G. J. & Poulos, T. L. (1996). Probing the cytochrome *c* peroxidase-cytochrome *c* electron transfer reaction using site specific cross-linking. *Biochemistry* **35**, 4837-4845.
13. Geren, L., Hahm, S., Durham, B. & Millett, F. (1991). Photoinduced electron transfer between cytochrome *c* peroxidase and yeast cytochrome *c* labeled at Cys102 with 4-bromomethyl-4'-methylbipyridine [bis bipyridine]ruthenium^{2+}. *Biochemistry* **30**, 9450-9457.
14. Miller, M. A., Liu, R. Q., Hahm, S., Geren, L., Hibdon, S., Kraut, J., Durham, B. & Millett, F. (1994). Interaction domain for the reaction of cytochrome *c* with the radical and the oxyferryl heme in cytochrome *c* peroxidase compound I. *Biochemistry* **33**, 8686-8693.
15. Mauro, J. M., Fishel, L. A., Hazzard, J. T., Meyer, T. E., Tollin, G., Cusanovich, M. A. & Kraut, J. (1987). Tryptophan-191->phenylalanine, a proximal-side mutation in yeast

cytochrome *c* peroxidase that strongly affects the kinetics of ferrocytochrome *c* oxidation. *Biochemistry* **27**, 6243-6256.
16. Poulos, T. L. & Kraut, J. (1980). The stereochemistry of peroxidase catalysis. *J. Biol. Chem.* **255**, 8199-8205.
17. MacGillavry, C. H. & Rieck, G. D. e., Eds. (1968). . Vol. III. International tables of crystallography. Birmingham, UK: Kynoch Press.
18. Hirst, J., Wilcox, S. K., Williams, P. A., Blankenship, J., McRee, D. E. & Goodin, D. B. (2001). Replacement of the axial histidine ligand with imidazole in cytochrome c peroxidase. 1. Effects on structure. *Biochemistry* **40**, 1265-1273.
19. Buzy, A., Bracchi, V., Sterjiades, R., Chroboczek, J., Thibault, P., Gagnon, J., Jouve, H. M. & Hydry-Clergeon, G. (1995). Complete amino acid sequence of *Proteus mirabilis* PR catalase. Occurrence of a methionine sulfone in the close proximity of the active site. *J. Protein. Chem.* **14**, 59-72.
20. Stehle, T., Ahmed, S. A., Clairbone, A. & Schultz, G. E. (1991). Structure of NADH peroxidase from *Streptococcus faecalis* 10C1 refined at 2.16 Å resolution. *J. Mol. Biol.* **221**, 1325-1344.
21. Heim, R., Prasher, D. C. & Tsien, R. Y. (1994). Wavelength mutation and posttranslational autooxidation of green fluorescent protein. *Proc. Natl. Acad. Sci. USA* **91**, 12501-12504.
22. Ormo, M., Cubitt, A. B., Kalio, K., Gross, L. A., Trien, R. Y. & Remington, S. J. (1996). Crystal structure of the *Aequorea victoria* green fluorescent protein. *Science* **273**, 1392-1395.
23. Hao, B., Gong, W. M., Ferguson, T. K., James, C. M., Krzycki, J. A. & Chan, M. K. (2002). A new UAG encoded residue in the structure of a Methanogen Methyltransferase. *Science* **296**, 1462-1466.
24. Ostermeier, C., Harrenga, A., Ermler, U. & Michel, H. (1997). Structure of 2.7 Å resolution of the Paracoccus denitrificans two-subunit cytochrome *c* oxidase complexed with an antibody F_V fragment. *Proc. Natl. Acad. Sci. USA* **94**, 10547-10553.
25. Yoshikawa, S., Shinzawa-Itoh, K., Nakashima, R., Yaono, R., Yamashita, E., Inoue, N., Yao, M., Fei, M. J., Libeu, C. P., Mizushima, T., Yamaguchi, H., Tomizaki, T. & Tsukihara, T. (1998). Redox-coupled crystal structural changes in bovine heart cytochrome *c* oxidase. *Science* **280**, 1723-1729.
26. Buse, G., Soulimane, T., Dewor, M., Meyer, H. E. & Bluggel, M. (1999). Evidence for a copper-coordinated histidine-tyrosine cross-link in the active site of cytochrome *c* oxidase. *Protein Sci.* **8**, 985-990.
27. Pinakoulaki, E., Pfitzner, U., Ludwig, B. & Varotsis, C. (2002). The role of the cross-link His-Tyr in the functional properties of the binucelar center in cytochrome *c* oxidase. *J. Biol. Chem.* **277**, 13563-13568.
28. Bravo, J., Fita, I., Ferrer, J. C., Ens, W., Hillar, A., Switla, J. & Lowlen, P. C. (1997). Identification of a novel bond between a histidine and the essential tyrosine in catalase HPII of Escherichia coli. *Protein Sci.* **6**, 1016-1023.
29. Ito, N., Philips, S. E. V., Yadav, K. D. S. & Knowles, Y. P. F. (1994). Crystal structure of a free radical enzyme, galactose oxidase. *J. Mol. Biol.* **238**, 794-814.
30. Parsons, M. R., Convery, M. A., Wilmot, C. M., Yadav, K. D. S., Blakeley, V., Corner, A. S., Philips, S. E. V., McPherson, M. J. & Knowles, P. F. (1995). Crystal structure of a quinoenzyme: Copper amine oxidase of *Escherichia coli* at 2.0 Å resolution. *Structure* **3**, 1171-1184.

31. Yamada, Y., Fujiwara, T., Sato, T., Igarashi, N. & Tanaka, N. (2002). The 2.0Å crystal structure of catalase-peroxidase from *Haloarcula marismortui*. *Nature Struc. Biol.* **9**, 691-695.
32. Erman, J. E., Vitello, L. B., Miller, M. A., Shaw, A., Brown, K. A. & J., K. (1993). Histidine 52 is a critical residue for rapid formation of cytochrome *c* peroxidase compound I. *Biochemistry* **32**, 9798-9806.
33. Mondal, M. S., Goodin, D. B. & Armstrong, F. A. (1998). Simultaneous voltammetric comparisons of reduction potentials, reactivities, and stabilities of the high-potential catalytic states of wild-type and distal-pocket mutant (W51F) yeast cytochrome *c* peroxidase. *J. Amer. Chem. Soc.* **120**, 6270-6276.
34. Jovanovic, S. V., Steenken, S. & Simic, M. G. (1991). Kinetics and energetics of one-electron-transfer reactions involving tryptophan neutral and cation radicals. *J. Phys. Chem.* **95**, 684-687.
35. Davies, K. J. A., Delsignore, M. E. & Lin, S. W. (1987). Protein damage and degradation by oxygen radicals II. Modification of amino acids. *J. Biol. Chem.* **262**, 9902-9905.
36. Long, B. H., Rose, W. C., Vyas, D. M., Matson, J. A. & Forenza, S. (2002). Discovery of antitumor indolocarbazoles: rebeccamycin, NSC 655649, and fluoroindolocarbazoles. *Curr. Med. Chem.: Anti-Cancer Agents* **2**, 156-266.
37. Gilbert, E., Chisholm, J. D. & Van Vranken, D. L. (1999). Conformational control in the rebeccamycin class of indolocarbazole glycosides. *J. Org. Chem.* **64**, 5670-5676.
38. Fishel, L. A., Villafranca, J. E., Mauro, J. M. & Kraut, J. (1987). Yeast cytochrome *c* peroxidase: mutagenesis and expression in *Escherichia coli* show tryptophan-51 is not the radical site in compound I. *Biochemistry* **27**, 351-360.
39. Choudhury, K., Sundaramoorthy, M., Hickman, A., Yonetani, T., Woehl, E., Dunn, M. F. & Poulos, T. L. (1994). Role of the proximal ligand in peroxidase catalysis. Crystallographic, kinetic, and spectral studies of cytochrome *c* peroxidase proximal ligand mutants. *J. Biol. Chem.* **269**, 20239-20249.
40. Edwards, S. L. & Poulos, T. L. (1990). Ligand binding and structural perturbations in cytochrome *c* peroxidase. A crystallographic study. *J. Biol. Chem.* **265**, 2588-2595.
41. Sundaramoorthy, M., Choudhury, K., Edwards, S. L. & Poulos, T. L. (1991). Crystal structure and preliminary functional analysis of the cytochrome *c* peroxidase His175Gln proximal ligand mutant. *J. Amer. Chem. Soc.* **113**, 7755-7757.
42. Otwinowski, Z. & Mino, V. (1997). Processing of X-ray diffraction data collected in oscillation mode*, Methods Enzymol.* **276**, 307-326.
43. Howard, A. J. (2000). *Data processing in macromolecular crystallography.* Crystallographic Computing 7: Proceedings
from the Macromolecular Crystallographic Computing School, 1996 (Watenpaugh, P. E. B. a. K. D., Ed.), Oxford University Press, Oxford.
44. Finzel, B. C., Poulos, T. L. & Kraut, J. (1984). Crystal structure of yeast cytochrome *c* peroxidase refined at 1.7 Å resolution. *J. Biol. Chem.* **259**, 13027-13036.
45. Brunger, A. T., Adams, P. D., Clore, G. M., DeLano, W. L., Gros, P., Grosse-Kunstleve, R. W., Jiang, J. S., Kuszewski, J., Nilges, M., Pannu, N. S., Read, R. J., Rice, L. M., Simonson, T. & Warren, G. L. (1998). Crystallography & NMR System: A New Software Suite for Macromolecular Structure Determination. *Acta Crystallogr.* **D54**, 905-921.

46. Brunger, A. T. (1992). Free *R* value: a novel statistical quantity for assessing ther accuracy of crystal structures. *Nature* **355**, 472-475.
47. Jones, T. A. (1985). Diffraction methods for biological macromolecules. Interactive computer graphics: *FRODO*. *Methods. Enzymol.* **115**, 157-171.
48. Navaza, J. (1994). *AMoRe*: an automated package for molecular replacement. *Acta. Cryst. A* **50**, 157-163.
49. Kraulis, P. J. (1994). MOLSCRIPT: a program to produce both detailed and schematic plots of protein structures. *J. Appl. Crystallogr.* **24**, 946-950.
50. Esnouf, R. M. (1997). An extensively modified version of MolScript that includes greatly enhanced coloring capabilities. *J. Mol. Graph. Model.* **15**, 132-134.
51. Merritt, E. A. & Bacon, D. J. (1997). Raster3D: photorealistic molecular graphics. *Methods Enzymol.* **277**, 505-524.

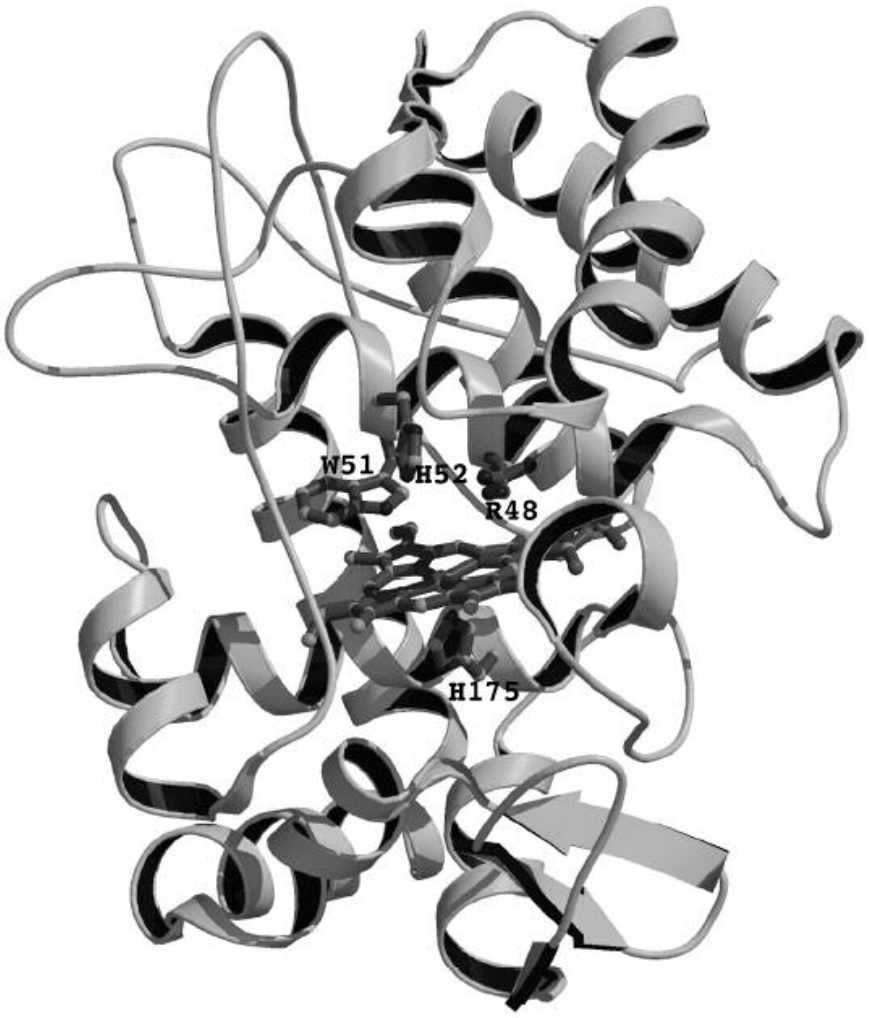

Fig. 1: Model of CcP showing key residues relevant to this study.

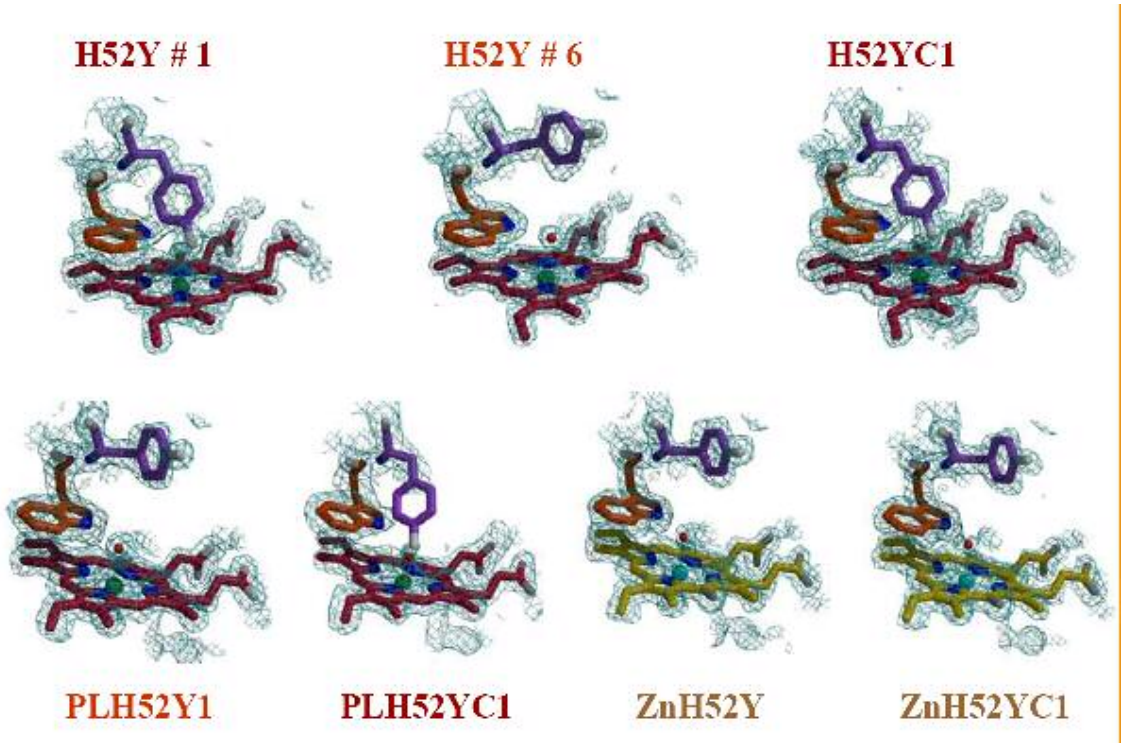

Fig. 2: $2F_o$-F_c omit electron density maps contoured at 1σ A) The original structure of the H52Y mutant where the Trp51-Tyr52 cross-link forms spontaneously. B) The H52Y mutant crystallized with fresh reagents. Here the cross-link does not form. C) Same as in C except a crystal was treated with peroxide and the cross-link does form. D) This map was generated from plate-like crystals and shows no cross-link. E) Same as in D except the crystal was treated with peroxide. F) The H52Y mutant with Zn-porphyrin. G) The same crystal used in panel F was thawed, treated with peroxide, and a second data set collected.

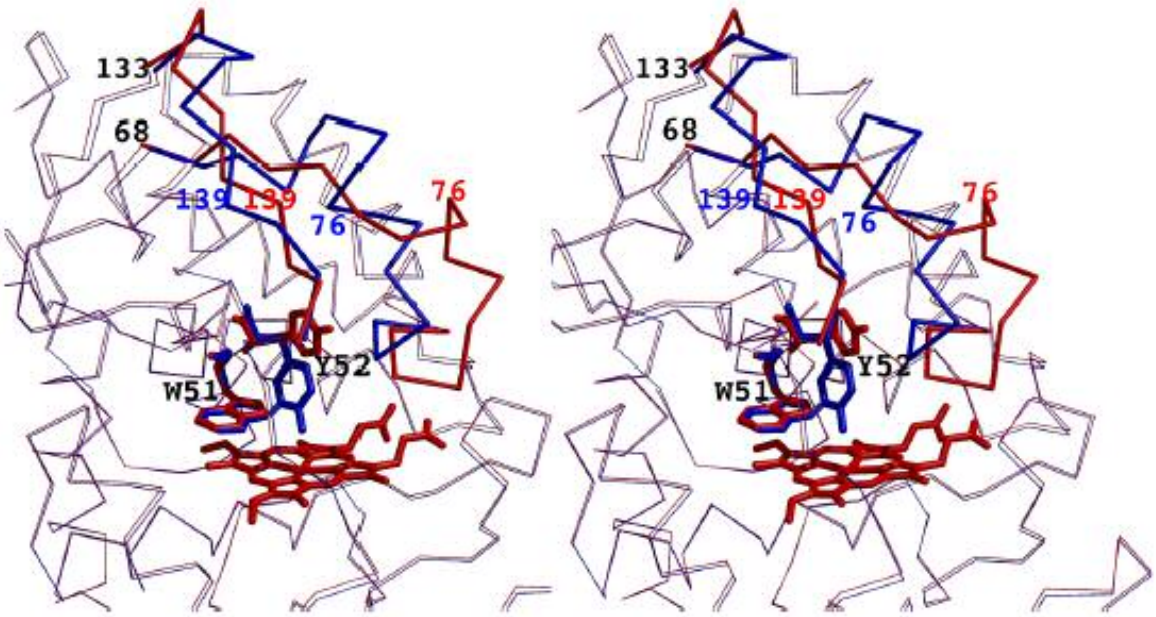

Fig. 3: Stereo models of the "*closed*" and "*open*" forms of the H52Y mutants. The "*closed*" is blue while the "*open*" which has undergone the conformational change is red. Those regions which undergo the most significant change in structure are highlighted as thickened lines.

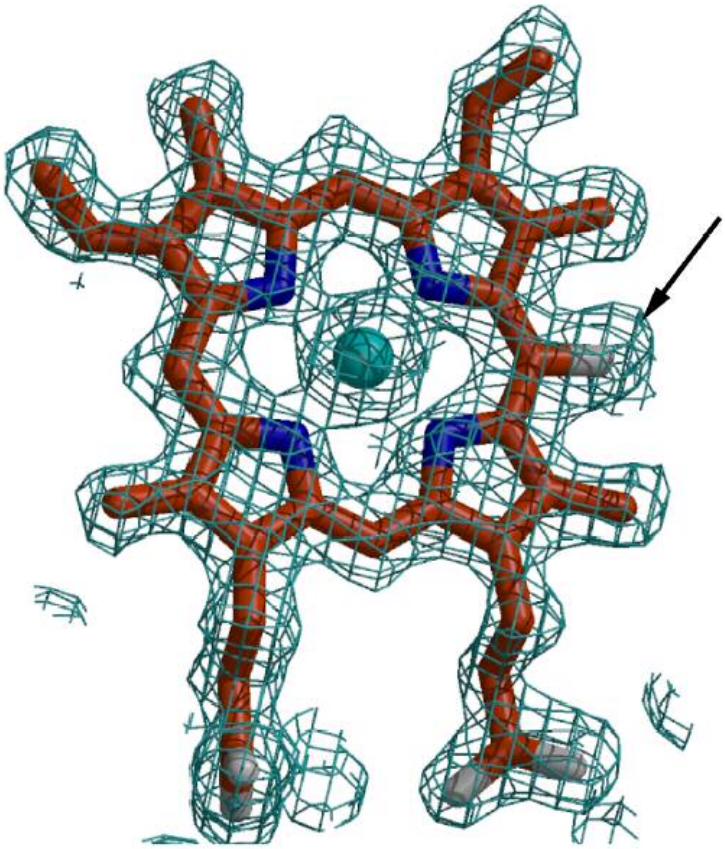

Fig. 4: $2F_o$-F_c omit electron density map contoured at 1 σ of the Zn-porphyrin. The arrow indicates the extra lobe of electron density, which we attribute to oxidation of δ-*meso* carbon of the protoporphyrin.

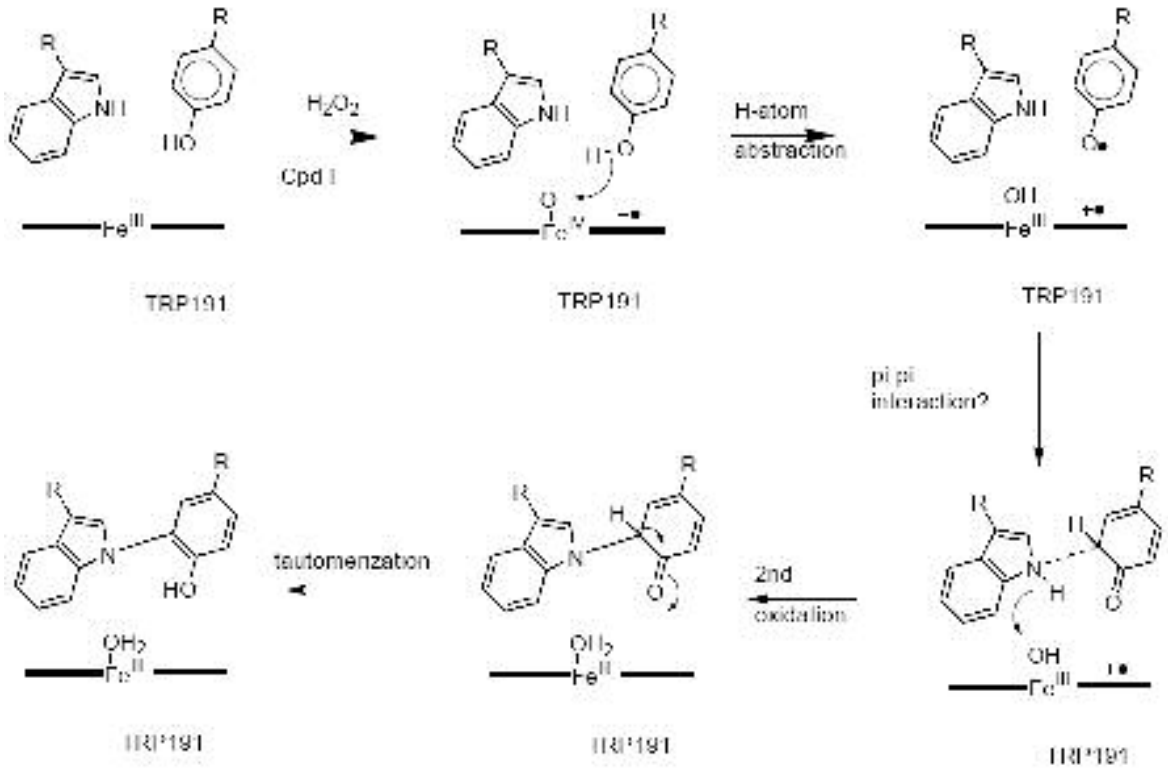

Fig. 5: Proposed reaction mechanism in forming the Trp-Tyr cross-link. The heme iron assists in the homolytic cleavage of the peroxide O-O bond thus generating oxygen radicals. These in turn abstract H atoms from the nearby Trp and Tyr side chains resulting in the Trp-Tyr cross-link.

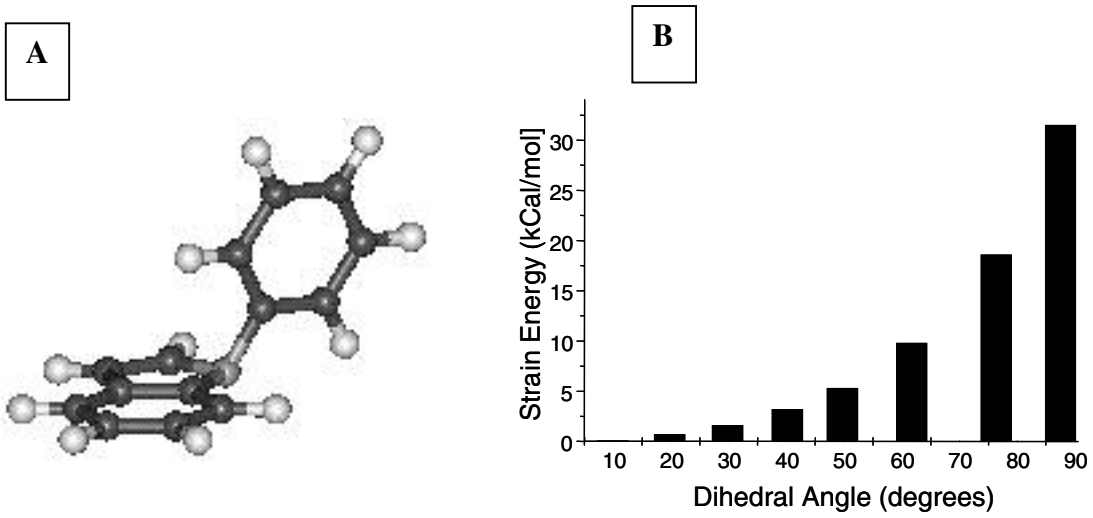

Fig. 6: **(A)** Indole-arene model used in calculating the strain energy due to bending of N-C cross-link bond; model shown at a dihedral angle of 60°. **(B)**Apparent strain ene rgy *vs*. N-C bond deformation, as measured by the change in calculated gas-phase energy as the angle between the indole and arene rings of the model are varied from 0 to 90°.

Table I: Data collection and refinement statistics of various H52Y proteins

	H52Y 1	H52Y6	H52Yper	PLH52Y	PLH52Yper	ZnH52Y	ZnH52Yper
PDB Code							
Crystal Data							
Space group	$P2_12_12_1$	$P2_12_12_1$	$P2_12_12_1$	$P2_12_12_1$	$P2_12_12_1$	$P2_12_12_1$	$P2_12_12_1$
Cell parameters (Å) $\alpha = \beta = \gamma$ (90°)	a = 106.773 b = 75.527 c = 51.033	a = 106.598 b = 75.943 c = 50.987	a = 106.828 b = 75.223 c = 51.043	a = 50.480 b = 50.957 c = 118.884	a = 50.465 b = 50.991 c = 118.525	a = 50.487 b = 50.998 c = 118.759	a = 50.485 b = 50.944 c = 118.774
Data Collection							
Resolution range (Å)	100.0 – 1.65	100.0 – 1.64	100.0 – 1.60	100.0 – 1.58	100.0 – 1.90	100.0 – 1.65	100.0 – 1.58
Total observations	434,660	673,145	305,303	627,338	515,341	434,384	834,365
Unique reflections	50,278	50,987	55,297	42,967	24,887	34,532	42,942
Completeness – all data (%)	99.40	97.20	97.60	94.80	89.30	91.20	89.30
R_{merge} (I)[1]	0.055	0.053	0.047	0.049	0.058	0.044	0.030
I/σ (I)	24.63	38.51	40.51	37.19	34.95	44.47	41.91
Redundancy – (%)	8.645	13.202	23.61	14.602	20.71	11.74	19.43
Last shell resolution - (Å)	1.68 – 1.65	1.67 – 1.64	1.63 – 1.60	1.61 – 1.58	1.93 – 1.90	1.68 – 1.65	1.61 – 1.58
Completeness (%)	98.20	77.90	88.50	87.90	93.20	86.80	85.90
R_{merge} (I)[1]	0.50	0.353	0.461	0.394	0.621	0.127	0.506
I/σ (I)	2.275	3.165	3.20	2.72	3.13	11.36	2.71
Refinement							
Resolution range - (Å)	50.0 – 1.65	50.0 – 1.64	50.0 – 1.60	50.0 – 1.58	50.0 – 1.90	50.0 – 1.65	50.0 – 1.58
Reflections (σI cutoff = 0)	48,421	49,436	53,697	40,622	22,178	34,380	38,231
R_{free}	0.1982 (4.8%)	0.2084 (4.9%)	0.2131 (4.9%)	0.2190 (4.8%)	0.2404 (4.3%)	0.2151 (4.6%)	0.2250 (4.5%)
R_{cryst}[2]	0.1798	0.1839	0.1926	0.1944	0.2025	0.1831	0.1960
RMS Deviation[3]							
Bond lengths (Å)	0.0049	0.0051	0.0063	0.0048	0.0056	0.0048	0.0049
Angle distances (°)	2.2416	2.174	2.27	2.245	2.196	1.18	1.28
Avg. protein B-factor (Å^2)	15.47	18.14	19.88	19.45	31.27	15.79	20.34
Avg. heme B-factor (Å^2)	11.96	13.23	15.67	13.61	22.47	11.91	16.39
Luzatti coordinate error (Å)	0.19	0.21	0.21	0.20	0.23	0.18	0.23
Water molecules	603	500	545	428	228	506	228

[1] $R_{merge} = \sum | I - \langle I \rangle | / \sum I$.

[2] $R_{cryst} = \sum (| F_{obs} | - | F_{calc} |) / \sum | F_{obs} |$. The R_{free} is the R_{cryst} calculated on the 5% reflections excluded for refinement

[3] r.m.s. bond and r.m.s. angle represent the root-mean-squared deviation between the observed and ideal values.